Review

Traditional and Iterative Group-IV Material Batteries through Ion Migration

Xiaojun He [1,2,3,†], Xiaoyan Wei [1,2,3,†], Zifeng Jin [1,2,3], Zhenglin Wang [1,2,3], Ya'nan Yang [1,2,3], Jinsheng Lv [1,2,3] and Nan Chen [1,2,3,*]

[1] Key Laboratory of Cluster Science, Ministry of Education of China, Key Laboratory of Photoelectronic/Electrophotonic Conversion Materials, School of Chemistry and Chemical Engineering, Beijing Institute of Technology, Beijing 100081, China; 3120221190@bit.edu.cn (X.H.); 3120221166@bit.edu.cn (X.W.); 3120231126@bit.edu.cn (Z.J.); 3120225589@bit.edu.cn (Z.W.); 3120205602@bit.edu.cn (Y.Y.); 3120211218@bit.edu.cn (J.L.)

[2] Yangtze Delta Region Academy, Beijing Institute of Technology, Jiaxing 314019, China

[3] Tangshan Research Institute, Beijing Institute of Technology, Tangshan 063000, China

* Correspondence: gabechain@bit.edu.cn

† These authors contributed equally to this work.

Abstract: In this review, we emphasize the significant potential of carbon group element-based (Group-IV) electrochemical energy devices prepared on the basis of ion migration in the realm of high-efficiency batteries. Based primarily on our group research findings, we elucidate the key advantages of traditional Group-IV materials as electrodes in ion batteries powered by metal ion migration. Subsequently, we delve into the operational principles and research progress of iterative Group-IV material moisture ion batteries, driven by ion migration through external moisture. Finally, considering the practical challenges and issues in real-world applications, we offer prospects for the development and commercialization of Group-IV materials utilizing ion migration in both conventional and next-generation battery technologies.

Keywords: carbon group (Group-IV) element; ion battery; moisture ion battery

1. Introduction

Ion migration refers to the process of ions moving within a medium driven by an external electric field or a chemical gradient. The prerequisite for the implementation of ion migration technology lies in the construction of suitable electrodes, electrolytes, and media [1–5]. Currently, ion migration technology is primarily applied in emerging energy storage and conversion devices [6–9]. Examples include supercapacitors, which store and release energy through charge adsorption and ion migration [10–19], and fuel cells based on ion exchange technology, where ions conduct for energy conversion [20–29]. In addition, ion batteries, based on the migration and insertion/extraction processes of ions in electrolytes and electrode materials, are among the most widely used and advanced energy storage devices.

Group-IV materials, due to their abundant raw materials, low production costs, non-toxic nature, and excellent electrochemical properties, serve as ideal anode materials for various ion migration-based batteries [30–32]. Over the past few decades, in addition to traditional amorphous carbon and graphite, various carbon materials like graphene and graphdiyne (GDY), as well as other Group-IV materials such as silicene, germanene, and tin have become well known. These materials not only differ in morphology and dimensions but also exhibit distinct local electronic structures [33–35]. Hence, a comprehensive understanding of the energy storage properties of various carbon materials still requires further research. Group-IV materials, as crucial components of ion migration-driven energy storage technologies, have been a focal point of research for decades. Various studies

encompass the design and fabrication of rational structures, as well as selecting metal ions with different valence states (Li^+, Na^+, K^+, Zn^{2+}, Mg^{2+}, Al^{3+}, etc.) to enhance the performance of ion batteries [36–42].

At the same time, exploring new mechanisms for ion migration-driven batteries is crucial for the application of battery technology in green, cost-effective, and large-scale energy storage and conversion [43,44]. In comparison to chemical energy storage systems in which ion batteries achieve energy conversion through ion migration, novel self-powered batteries based on carbon materials have gradually emerged through external stimuli, with moisture-enabled electricity generation (MEG) being the most significant among them [45]. This technology, serving as an innovative green energy harvesting technique, harnesses the interactions between carbon materials and ubiquitous atmospheric moisture to directly generate electrical energy. The electricity generation process relies on the dynamic adsorption and desorption of moisture and the migration of ions. Since moisture serves as the sole external source, this electricity generation process is highly environmentally friendly, with no pollutants produced, and is highly reversible. It can be viewed as an efficient, green, ion migration-driven battery for the next generation.

2. Traditional Group-IV Material Ion Batteries

2.1. Monovalent Alkali Metal Ion Batteries Assembled with Carbon Electrodes

Alkali metal ion batteries have garnered significant attention from scholars both domestically and internationally in recent years due to their promising prospects in large-scale electrochemical energy storage. Carbon materials, exemplified by graphene and carbon nanotubes, stand out for their unique structural characteristics, offering excellent conductivity and environmentally friendly, non-toxic attributes. These qualities make them essential electrode materials for the negative terminals of alkali metal ion batteries. The most representative alkali metal ionic batteries include lithium-ion batteries (LIBs), sodium-ion batteries (NIBs), and potassium-ion batteries (KIBs). Among these, LIBs were the first to be commercialized and are known for their higher capacity and power density compared to other early commercial batteries. Research focused on optimizing ion battery performance using carbon electrodes has gained significant attention.

Porous carbon materials have attracted widespread attention in the field of LIBs due to their high specific surface area, pore volume, low density, and excellent chemical stability, especially their multi-level pore size advantages [46]. When used as the anode in LIBs, their high specific surface area allows them to accommodate a greater number of lithium ions, providing high capacity for LIBs. Wang et al. [47] fabricated porous carbon with a substantial specific surface area through the direct carbonization of bovine bone at 1100 °C. This process yielded PC-1100, a highly defective porous carbon material, which demonstrated remarkable attributes: a specific surface area of 2096 $m^2\ g^{-1}$, a maximum mesopore volume of 1.829 $cm^3\ g^{-1}$, a tightly distributed mesopore size around 4.0 nm, and excellent electrical conductivity at 5141 S m^{-1}. In their research, PC-1100 was assessed as a negative electrode in LIBs, showcasing an impressive reversible capacity of 1488 mAh g^{-1} after 250 cycles at 1 A g^{-1}, and 661 mAh g^{-1} after 1500 cycles at 10 A g^{-1}. The multi-dimensional complex pore structure offers effective pathways for the diffusion of lithium ions and shorter distances for lithium ion diffusion. In a related study, Qu et al. [48] introduced a method for synthesizing two-dimensional (2D) stratified porous carbon (HPC) using soft asphalt as a carbon source, oyster shell as a template, and an activated precursor. When employed as an electrode material in LIBs, HPC demonstrated a remarkable reversible capacity of 1251 mAh g^{-1} at 0.1 A g^{-1} and exhibited outstanding cyclic stability. These findings underscore the effectiveness of the 2D layered structure in shortening the solid-state diffusion distance of lithium ions during the charge and discharge processes of LIBs. Defects such as vacancies and doping with heteroatoms can serve as sites for lithium storage. Liu et al. [49] introduced an efficient method for synthesizing Co_n@N-C hybrids (i.e, Co@N-C-0, Co_n@N-C-1, and Co_n@N-C-2), characterized by interconnected porous carbon nanostructures and numerous active sites like Co-N-C. When evaluated as

an anode material for LIBs, Co$_n$@N-C-1 showed remarkable lithium storage performance, starting with an initial reversible capacity of 1587 mAh g^{-1} at 0.1 C and maintaining a high reversible capacity of 1000 mAh g^{-1} at 5 C after 800 cycles. Both experimental and theoretical results validate the significant role of Co-N-C, with its high specific activity, in facilitating the transport and storage of Li$^+$ within interconnected porous carbon nanostructures. Consequently, porous carbon demonstrates superior electrochemical properties compared to conventional graphite carbon and has found successful application in ion batteries. As a result, porous carbon often exhibits better electrochemical performance than traditional graphite carbon and has been successfully applied in ion batteries.

Carbon nanotubes (CNTs) consist of single or multiple coaxial layers of carbon sheets, forming a material with a microstructure akin to that of graphite layers. This intricate microstructure enables a shallow penetration of alkali metal ions, shorter migration distances, and multiple insertion sites (including gaps and interlayer spaces) within the tubes and between the layers [50–52]. Moreover, due to the excellent electrical conductivity of CNTs and doped CNTs, they exhibit robust electronic conduction and efficient ion transport capabilities, thus establishing them as exemplary anode materials for LIBs. For example, Peng et al. [53] meticulously documented the development of vertically aligned nitrogen-doped core-sheath carbon nanotube (N-CNT) films for use as flexible anodes in LIBs (Figure 1a). These N-CNT films exhibited outstanding tensile strength (690 MPa) and electrical conductivity (410 S cm^{-1}). Furthermore, even under the demanding conditions of a 4C rate, these films displayed exceptional high capacity of 390 mAh g^{-1}, retaining 97% of this capacity after enduring 200 cycles. This highlights the advantages of carbon nanotubes in LIBs.
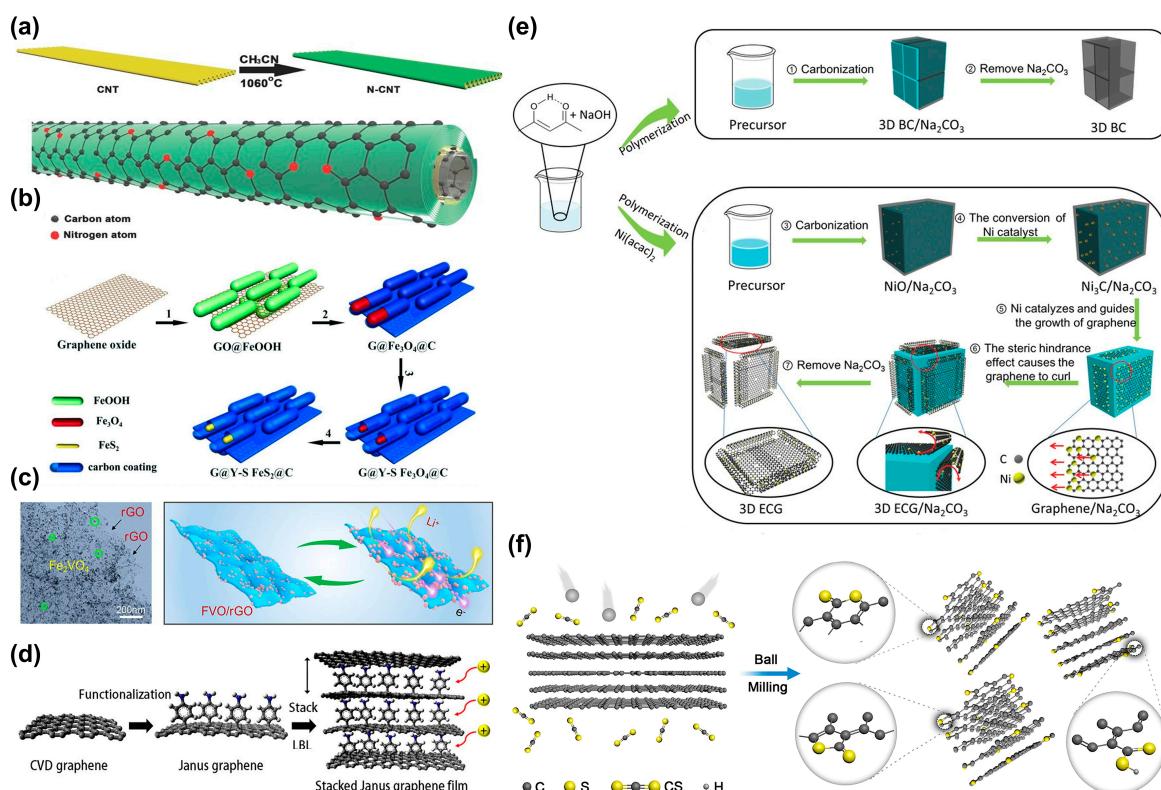

Figure 1. (**a**) Schematic illustration of the synthesis of the aligned N-CNT film and structure of an N-CNT. (**b**) Uniform small Fe$_2$VO$_4$ nanoparticles (FVO) are grown on reduced graphene oxide (rGO). (**c**) Schematic illustration of the preparation of the Janus graphene and the stacked Janus graphene thin film. (**d**) Schematic representation of the mechanochemical synthesis of TAGnPs via ball-milling graphite in the presence of carbon disulfide (CS$_2$). (**e**) Schematic illustration for the synthesis of G@Y-S FeS$_2$@C composite. (**f**) Schematic illustration of the synthesis process of 3D BC and 3D ECG.

Typical carbon electrodes include a 2D structure composed of carbon atoms, with graphene as a representative example. Graphene exhibits a high lithium storage capacity and an open porous structure that offers a low-energy barrier pathway for electrolyte ions, ensuring excellent rate capability [54,55]. Baek et al. [56] prepared edge-functionalized graphene nanosheets (GnPs) with thiolactic acid (TA) via a ball-milling method (Figure 1f). These GnPs exhibited a low average working voltage (<0.5 V) and exceptional rate performance (>0.5 A g^{-1}) as an anode material for LIBs. Researchers believe that the high specific capacity of graphene primarily arises from the presence of abundant edge defects and excellent electrical conductivity, resulting in an electrode film resistance of only 10~1000 Ω sq^{-1}. Therefore, designing specific microstructures of graphene holds significant importance for enhancing the specific capacity of LIBs. Sun et al. [57] introduced a novel method for producing 3D edge-curled graphene (3D ECG) and conducted half-cell tests using lithium to demonstrate its outstanding electrochemical performance (Figure 1e). The specific capacities measured were 907.5 mAh g^{-1} at a current density of 0.05 A g^{-1} and 347.8 mAh g^{-1} at 5.0 A g^{-1}. Similar to graphene, GDY shares hybrid carbon atoms and boasts a distinctive p-conjugated carbon framework with a 2D expanded structure. Huang et al. [58] synthesized chlorographdiyne (Cl-GDY) through a Glaser–Hay coupling reaction on copper foil. This bottom-up preparation of Cl-GDY, combined with its robust chemical functionalization capability using alkyl monomers, yields a carbon skeleton with a substantial and evenly distributed presence of substituted chlorine atoms. These chlorine atoms possess suitable electronegativity and atomic size, enabling them to collaboratively and steadfastly accommodate lithium within the Cl-GDY skeleton. Consequently, this process creates a greater number of lithium storage sites. With the increasing commercialization of ion batteries, there is a growing interest in NIBs and KIBs due to cost-effectiveness and raw material availability considerations. The unique structural characteristics of carbon electrodes offer effective solutions to the challenges posed by the larger atomic radii and higher relative molecular mass of sodium and potassium ions. For instance, Xu et al. [59] developed a composite material with a yolk-shell structure (G@Y–SFeS$_2$@C) on a graphene substrate (Figure 1b), incorporating FeS$_2$. This composite material offers excellent electrical conductivity and ample internal void space to accommodate the volume expansion of FeS$_2$. Palermo et al. [60] reported the fabrication of a nanostructured graphene anode for Na$^+$ storage, which includes Janus graphene, featuring functionalized stacked graphene sheets on one side (Figure 1d). Zhang and co-workers uniformly grew Fe$_2$VO$_4$ nanoparticles (FVO) on highly conductive reduced graphene oxide (rGO) through solvent-thermal treatment followed by annealing (Figure 1c). This resulted in the formation of a conductive network (FVO/rGO) conducive to Na$^+$ migration and storage [61]. GDY, as a representative 2D carbon material, also plays a pivotal role in enhancing NIBs and KIBs, owing to its distinctive conjugated structure. Sun et al. [62] employed first principle calculations to estimate the intrinsic storage capacity of potassium ions in GDY, revealing a remarkably high value of up to 620 mAh g^{-1}, a substantial improvement compared to graphite's capacity of 278 mAh g^{-1}. Subsequent experimental evaluations confirmed the outstanding electrochemical performance of the prepared GDY framework when used as a KIB anode, exhibiting a robust specific capacity of approximately 505 mAh g^{-1} at 50 mA g^{-1}. Additionally, it demonstrated exceptional rate capability (150 mAh g^{-1} at 5000 mA g^{-1}) and impressive cycle stability, with a capacity retention rate exceeding 90% after 2000 cycles at 1000 mA g^{-1}. Huang et al. [63] designed a sodium-ion electrode based on unique conjugated structure of boron-GDY. Boron-GDY boasts a distinctive conjugated structure, featuring an sp-hybrid carbon skeleton and uniformly distributed boron heteroatoms on the 2D molecular plane. The unconventional bonding environment created by the full sp-carbon framework and the electron-deficient boron centers enhances the affinity for metal atoms, thereby offering additional binding sites for efficient ion storage. Furthermore, the expanded molecular pore within the Boron-GDY molecular plane facilitates the vertical transfer of metal ions, further improving its performance as an electrode material. This exemplifies another typical application of GDY and its derivatives in ion

batteries. In addition to conventional graphene and GDY, other carbon materials with porous structures have notably enhanced the performance of low-valence ion batteries. Lu et al. [64] introduced a layered structure of nitrogen-doped carbon microspheres (CMSs). This structure not only offers more active sites but also mitigates the volume expansion caused by potassium ion insertion. As an anode material for PIBs, CMSs demonstrated impressive reversible discharge capacities of 328 and 125 mAh g^{-1} at 100 and 3000 mA g^{-1}, respectively. Furthermore, Lu et al. [65]. developed a $MoSe_2$/N-C KIB using 1 M potassium bis(fluoro-sulfonyl) imine in ethyl metal carbonate as an electrolyte. The negative electrode material comprises a MoSe2/N-C composite coated with carbon-coated $MoSe_2$ nanosheets. K^+ insertion induces a phase transition in $MoSe_2$, leading to the formation of $Mo_{15}Se_{19}$ during charging and K_5Se_3 as the final discharge product. After 300 cycles at 100 mA g^{-1}, the $MoSe_2$/N-C KIBs exhibited a reversible capacity of 258.02 mA h g^{-1}, with a Coulombic efficiency close to 100%. This showcases excellent rate performance and long-cycle stability.

2.2. Multivalent Metal-Ion Batteries Assembled with Carbon Materials

The relative scarcity of metal resources, with lithium as a representative, and their uneven global distribution have constrained the rapid development of monovalent metal-ion batteries. Therefore, the development of low-cost, high-safety, and high-energy-density carbon-based ion batteries is crucial for the future of energy storage. Multivalent metal batteries, such as magnesium ion batteries, zinc ion batteries, and aluminum ion batteries, have emerged in recent years as highly promising next-generation secondary batteries.

Magnesium ion batteries using carbon electrodes have brought new possibilities for battery technology due to their high bulk energy density and absence of dendrite problems. The use of carbon electrodes in magnesium ion batteries has opened up exciting possibilities in battery technology. These carbon materials, particularly graphene, a 2D nanomaterial, have proven effective in addressing dendrite-related issues during ion migration in magnesium ion batteries. In their research, Xu et al. [66] utilized fluorine-doped graphene nanosheets (FGS) as electrode materials for MIBs (Figure 2a). They observed that the FGS electrode exhibited a specific capacity of 100 mAh g^{-1} at a current density of 10 mA g^{-1} when cycled from 0.5 V to 2.75 V in $MgClO_4$-DMSO electrolyte. This unique Mg/FGS system operates through a preceding anion process, followed by reversible cation storage. The reduction in charge density due to the formation of large-sized monovalent complex cations and the easy accessibility to surface redox sites contribute to minimal voltage polarization, with minimal MgF_2 nucleation. The distinctive structure of carbon materials not only facilitates ion migration but also provides a platform for coating and supporting other materials, thereby enhancing material conductivity and optimizing magnesium ion battery performance. In a separate study by Chi et al. [67], a cathode material for MIBs was developed using nickel-doped titanium dioxide bronze coated with redox graphene and carbon nanotubes (rGO@CNT) (Figure 2b). At a current density of 100 mA g^{-1}, the discharge specific capacity of NT-2/rGO@CNT reached an impressive 167.5 mAh g^{-1}, which is 2.36 times that of pure TiO_2-B. Another notable development is the use of a binder-free polyaniline array/carbon cloth (PANI/CC) as the electrode material for MIBs by An et al. [68], as shown in Figure 2f. The incorporation of carbon cloth significantly enhances the electrode's conductivity and mitigates ion agglomeration. Comparatively, this electrode exhibits improved chemical performance when compared to a pure PANI electrode. The PANI/CC cathode demonstrates the highest specific capacity of 219 mA h g^{-1} at 200 mA g^{-1}, with an outstanding capacity retention rate of 97.25% even after more than 1500 cycles at 1 A g^{-1}.

Combining zinc ions with carbon electrodes to fabricate ion batteries highlights the potential of this technology due to its low manufacturing cost, enhanced safety, and excellent recyclability [69–71]. Especially in Zinc-ion batteries (ZIBs), the use of water electrolytes has shown great potential for portable electronic applications and large-scale energy storage systems. Our group has also achieved some important results in this regard. Qu et al. [72] prepared in situ cathode materials for water-containing fast-charging and ultra-stabilized

Zn-I_2 batteries, which exhibited a capacity of 90 mAh g^{-1} at 5 A g^{-1} and a superior long-cycle life close to 39,000 cycles with a capacity retention of 80.6% after a series of rate tests from 0.2 to 5 A g^{-1}. This excellent performance is attributed to the ideal mesoporous carbon structure, which shortens the ionic and electronic diffusion paths and can confine the polyiodide compound/iodine conversion reaction inside the mesopore (Figure 2e). In addition, carbon materials not only provide traditional optimization strategies but also bring new hope for the development of intelligent ion batteries. For example, Qu et al. [73] have designed a powerful Zn-air battery, utilizing a graphene-coated sponge as a pressure-sensitive air cathode (Figure 2c), enabling the ion battery to autonomously control energy output.
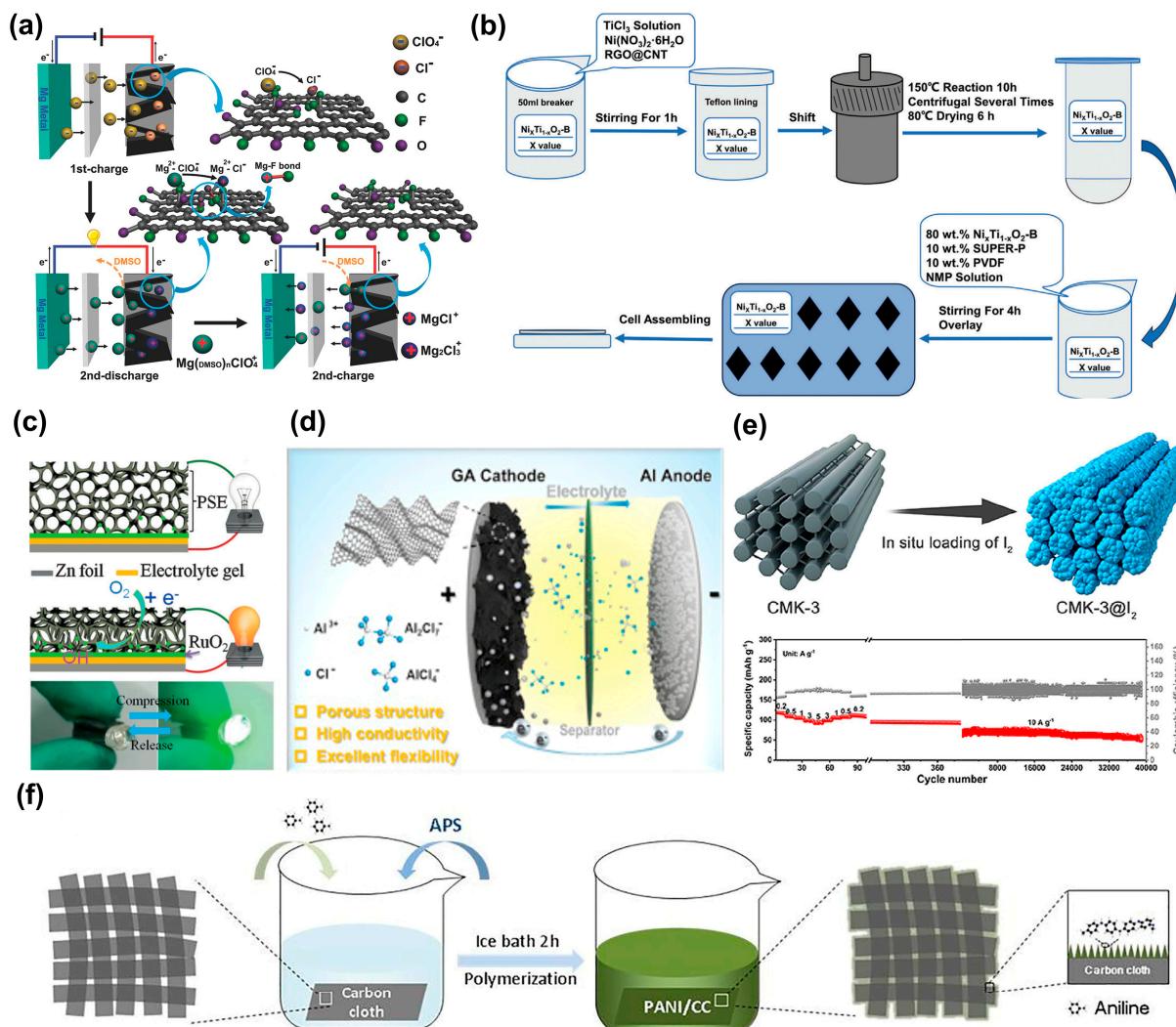

Figure 2. (**a**) Scheme of electrochemical reaction mechanisms of a Mg/FGS battery involving multiple (complex) cation or anion (de)intercalations during the early cycles. (**b**) Diagram of preparation of Al/GA-B. (**c**) Schematic structure and working principle of TSB under compression. (**d**) Polyaniline/CC material preparation schematic diagram. (**e**) Schematic illustration of the preparation of CMK-3@I_2. (**f**) Schematic of preparation strategy of $Ni_xTi_{1-x}O_2$-B/rGO@CNT composite.

Aluminum-ion batteries (AIBs) have garnered significant interest due to their higher valency, cost-effectiveness, and non-flammable nature. Nonetheless, akin to other ion-based batteries, the transport and storage of Al^{3+} within the electrode material pose formidable challenges, impeding the advancement of Al-ion batteries. Carbon materials present a promising avenue for enhancing Al-ion battery performance due to their distinctive structure. As an illustration, Wu et al. [74] demonstrated the facile fabrication of nanoporous,

densely stacked films using three-dimensional (3D) graphene aerogel (Figure 2d). This was achieved through the rapid reduction of GO aerogel via self-propagating combustion within a matter of seconds. This material was employed as an advanced, binder-free cathode for high-capacity AIBs with ultra-fast performance. Owing to the exceptional attributes of the graphene aerogel-derived dense film, including its 3D nanoporous structure, substantial surface area (513 m^2 g^{-1}), high electrical conductivity (581 S cm^{-1}), dense packing (0.61 g cm^{-3}), and expanded interlayer spacing (3.69 Å), the assembled AIBs exhibited a significantly higher capacity (245 mAh g^{-1}) at 1 A g^{-1}, surpassing that of AIB graphite by a factor of two. Furthermore, Yu et al. [75] introduced a thermal reductive perforation TRP method. In this procedure, the thermal decomposition of the block copolymer generates reactive radicals that react with oxygen, resulting in the production of graphene fragments. This material exhibits a three-layer structure with in-plane nanopores, an interlayer spacing expanded by over 50%, and oxygen content similar to that of graphene following high-temperature annealing. When employed as an AIB cathode, it achieved a reversible capacity of 197 mAh g^{-1} at a current density of 2 A g^{-1}, representing 92.5% of the theoretical capacity projected by density flood theory simulations. Cai et al. [76] synthesized a composite of converted FeF_3-expanded graphite (EG) with favorable electrical conductivity and cyclability for use as a cathode material in AIBs. The enhanced interaction between expanded graphite and FeF_3 resulted in increased electrical conductivity of FeF_3, improving interfacial charge transfer and boosting the thermodynamics and kinetics of FeF_3 nanoparticles for Al^{3+} insertion. As a result, the AIB demonstrated a satisfactory reversible specific capacity of 266 mAh g^{-1} at 60 mA g^{-1} after 200 cycles, along with a Coulombic efficiency of nearly 100% after 400 cycles at a current density of 100 mA g^{-1}.

Moreover, beyond single-metal ion batteries, there are bimetallic ion batteries, such as Li^+/Mg^{2+} hybrid-ion batteries (LMIBs), which combine the advantages of LIBs and MIBs. Zhao et al. [77] presented an oxygenated MoS_2 nanoconjugation (O-MoS_2/G) anchored on graphene. Their study demonstrated that the intercalation behavior of Li^+ facilitates the intercalation kinetics of Mg^{2+}, and the insertion of Li^+ into MoS_2 reduces the Mg^{2+} migration energy barrier. The O-MoS_2/G exhibited superior rate capability and cycling performance, maintaining a reversible capacity of 123.3 mAh g^{-1} after 2000 charge–discharge cycles at 1000 mA g^{-1}.

2.3. Metal-Ion Batteries Assembled with Other Group-IV Materials

At present, the reversible specific capacity of C negative electrode materials is close to the theoretical specific capacity of 372 mAh g^{-1}. Therefore, in order to improve the energy density of LIBs, it is necessary to develop negative electrode materials with higher specific capacity. Materials based on Group-IV elements (Si, Ge, Sn) possess high capacity, and extensive research has been conducted on their utilization as replacements for carbon-based electrodes in ion batteries.

Elemental Si and C share similar structures and chemistry, making materials like siloxane, akin to graphene, a valuable choice in designing electrodes for ion batteries. The key to silicon-based materials is nano-dispersion, such as the preparation of nanosheets of silicon, which effectively reduces surface stresses and thus alleviates volume expansion problems. Feng et al. [78], for instance, developed 2D pre-lithiated siloxane nanosheets with a high Initial Coulombic Efficiency (ICE) for use as lithium-ion anodes (Figure 3a). These nanosheets were obtained through chemical pre-lithiation and demonstrated a meticulously controlled uniform layered structure. Subsequently, by immersing the anode in a lithiation reagent, they generated siloxanes with a high ICE. They assembled a high-energy-density battery by using a pre-lithiated siloxane anode and a 5 V-class $LiNi_{0.5}Mn_{1.5}O_4$ cathode, which exhibited improved cycling performance and retained 94.3% of its capacity after 200 cycles.

The silicon electrode typically undergoes significant volumetric changes (ranging from 300% to 400%) during the metal ion insertion/extraction process. Consequently, this leads to the pulverization of the active material, continuous generation of the solid electrolyte

interface (SEI) layer, poor contact between the active material and the current collector, as well as a low initial Coulombic efficiency (ICE). These severe deteriorations have a substantial impact on the practical application of silicon negative electrodes. Lou et al. [79] engineered freestanding silicon-graphene electrodes, known as 3D-printed grid-like silicon-graphene (3D-Si/G) electrodes, through the use of 3D printing technology to control the electrode's structure (Figure 3b). This innovative design integrated numerous layered pores and 3D porous scaffolds, effectively addressing volume expansion and contraction concerns linked to silicon anodes. Additionally, the rGO network expedited electron-ion transfer, accelerating electrochemical reaction kinetics. Consequently, the optimized 3D-Si/G-1 electrode achieved an exceptionally high surface capacity of 16.2 mAh cm^{-2}.
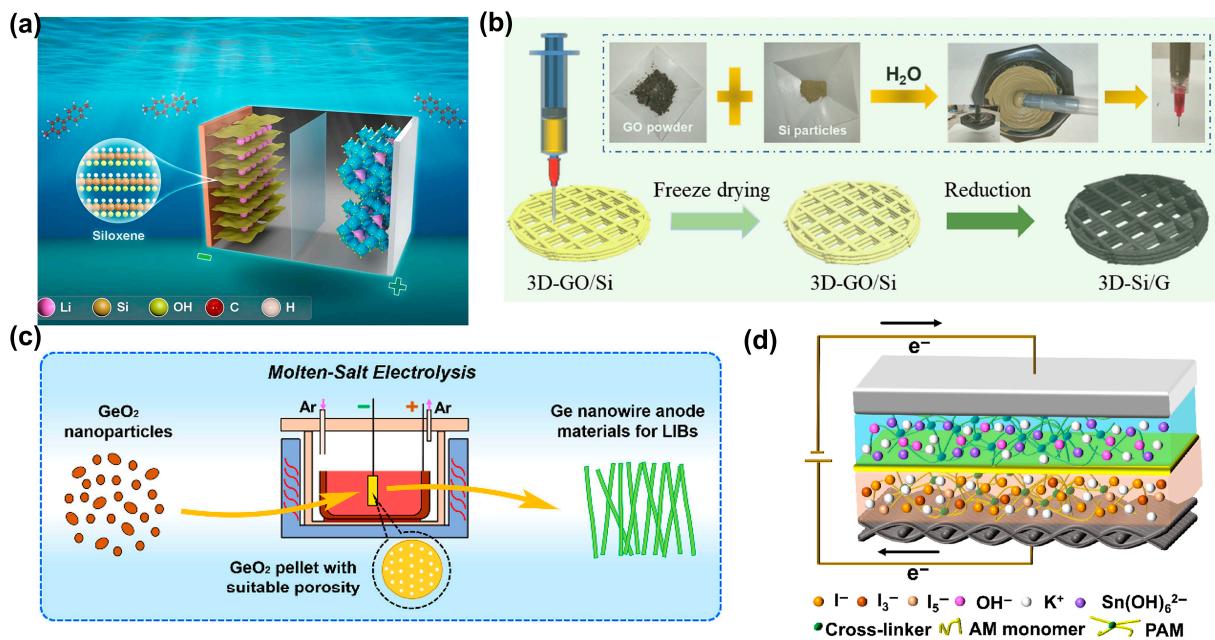

Figure 3. (**a**) Schematic diagram of the mechanism of prelithiated 2D siloxane nanosheets as anode for LIBs. (**b**) The schematic diagram of the preparation process of the 3D-Si/G electrode (the inset is the preparation process of the GO-Si ink). (**c**) A LIB anode: preparation of germanium nanowires by molten salt electrolysis. (**d**) The mechanism is schematic of a quasi-solid aqueous tin-iodide battery with tin foil as the anode, carbon cloth as the cathode and gel electrolyte as the material.

Furthermore, less researched but highly theoretical capacity materials from the other Group-IV materials, including germanium and tin-based electrode materials, have emerged as the most promising alternatives to carbon-based electrode materials for the future. For instance, Zhang et al. [80] introduced a novel approach for producing germanium (Ge) nanowires as anode materials for LIB, utilizing molten salt electrolysis (Figure 3c). The optimized Ge nanowires exhibited an impressive capacity of 1058.9 mAh g^{-1} at 300 mA g^{-1}, and they maintained over 602.5 mAh g^{-1} at 3000 mA g^{-1} through 900 cycles. Moreover, batteries have been designed to utilize elemental tin directly as a source of migrating ions. A notable example is the quasi-solid aqueous tin-iodine battery pioneered by Qu et al., [81] featuring tin foil as the positive electrode, carbon cloth as the negative electrode, and a gel electrolyte (Figure 3d). The anode underwent reversible conversion from $K_2Sn(OH)_6$ to metallic Sn, effectively eliminating the formation of metallic dendrites. Simultaneously, the gel electrolyte mitigated anode corrosion and enhanced anode utilization. Consequently, the prepared quasi-solid-state battery achieved a remarkable areal capacity of 700 μAh cm^{-2} (equivalent to the theoretical capacity of 211 mAh g^{-1}) and exhibited robust cycling stability, with no significant capacity loss even after 120 cycles at 1 mA cm^{-2}. Group-IV elements play a pivotal role in ion battery design, serving both to enhance conventional ion batteries

due to their unique structures and as a foundational platform for research, paving the way for pioneering new ion battery technologies.

3. Iterative Group-IV Materials Ion Batteries

In recent years, in response to the energy crisis, people have been continuously exploring environmentally friendly ways of obtaining green energy. Simultaneously, the rapid development of smart energy storage devices and energy conversion equipment has brought about significant challenges [82,83]. Consequently, individuals have begun seeking available sources of energy from the environment. Moisture ion battery technology, as an iterative nergy battery based on ion migration, is garnering increasing attention from scientists. It primarily relies on ion orderly migration induced by the moisture ion effect. When carbon-based materials come into contact with moisture, solvent effects cause directed ion migration within the material, thereby generating moisture-enabled electricity (ME). We refer to this type of ion migration-based power generation battery as a moisture ion battery, which is an innovation from our group [84].

The moisture ion batteries have made significant technological advancements. For instance, moisture ion power generation has expanded to include various materials, progressing from initial graphene to materials such as GDY and others. The power generation mechanism of moisture ion batteries is also gradually being refined. Many researchers have recognized the significant influence of the valence states of mobile ions on electrical signal generation. As a result, the primary mobile ions in moisture ion batteries have evolved from initially being hydrogen ions to the directed migration of high-valence ions. In summary, it is evident that moisture is the sole external source for these materials, and the process of ME is environmentally friendly, producing no polluting byproducts. Hence, it stands as an efficient green energy harvesting technology.

3.1. Moisture Hydrogen Ion Batteries

GO, a derivative of graphene, exhibits a substantial surface area, high intensity, ease of modification, and favorable biocompatibility. Notably, GO's surface is rich in functional groups, including -OH and -COOH, which confer diverse properties upon it. Qu et al. [84] investigated the utilization of this material in moisture hydrogen ion batteries (MHIBs). Figure 4a illustrates a typical preparation method, involving a freeze-drying technique to yield 3D materials with well-distributed pores from a GO solution (Figure 4b). Subsequent compression enhances the mechanical properties (Figure 4c). Furthermore, they introduce an oxygen gradient within the material via polarization. To assess the device's response to ambient humidity, they employ Al electrodes as upper and lower contacts, clamping the material between them (Figure 4d). The results depicted in Figure 4e reveal a gradual increase in voltage with rising relative humidity (RH). Notably, the findings are consistent with the expectation that the voltage can reach 0.3 V, and the current density can attain 3.5 mA cm^{-2} at 80% relative humidity (Figure 4e). Additionally, Yang et al. [85] utilize partially rGO as the ME material, integrated with machine learning (Figure 4f) to design devices capable of distinguishing diverse linguistic signals. Simultaneously, these devices have the capability to display and audibly communicate on smartphones, facilitating effective communication for individuals facing language barriers (Figure 4g). In summary, this research holds substantial potential for enhancing sustainable power systems.

Besides graphene, researchers are exploring the use of carbon based polymers in MHIBs. Qu et al. [86] utilized polycation (PDDA) and polyanion (PSSA) to create the MHIB, capable of generating electricity via the ME effect (Figure 4h). In contrast to conventional MHIBs, they incorporated active nanoaluminum components into the PSSA side. Due to its compact size, the battery meets the power requirements of small electronic devices. Figure 4h illustrates the composition of the MHIB unit, comprising PSSA, PDDA, and asymmetric electrodes. The positive electrode consists of PDDA-C on one side, while the negative electrode comprises PSSA on the side adjacent to the C-Al composite electrode. Consequently, a mere 0.3 cm^2 MEGs unit can produce an open-circuit voltage (V_{oc}) of up to

1.1 V (Figure 4i). An important factor contributing to the high output performance is the incorporation of active nano-components into the negative electrode. Aluminum (Al) can react with hydrogen ions, resulting in a substantial enhancement of the electrical signal. Furthermore, by employing straightforward series-parallel processing, this battery can readily provide power to electronic watches and weighing meters. These findings demonstrate the considerable industrial potential and broad applicability of this environmentally friendly battery (Figure 4j,k).
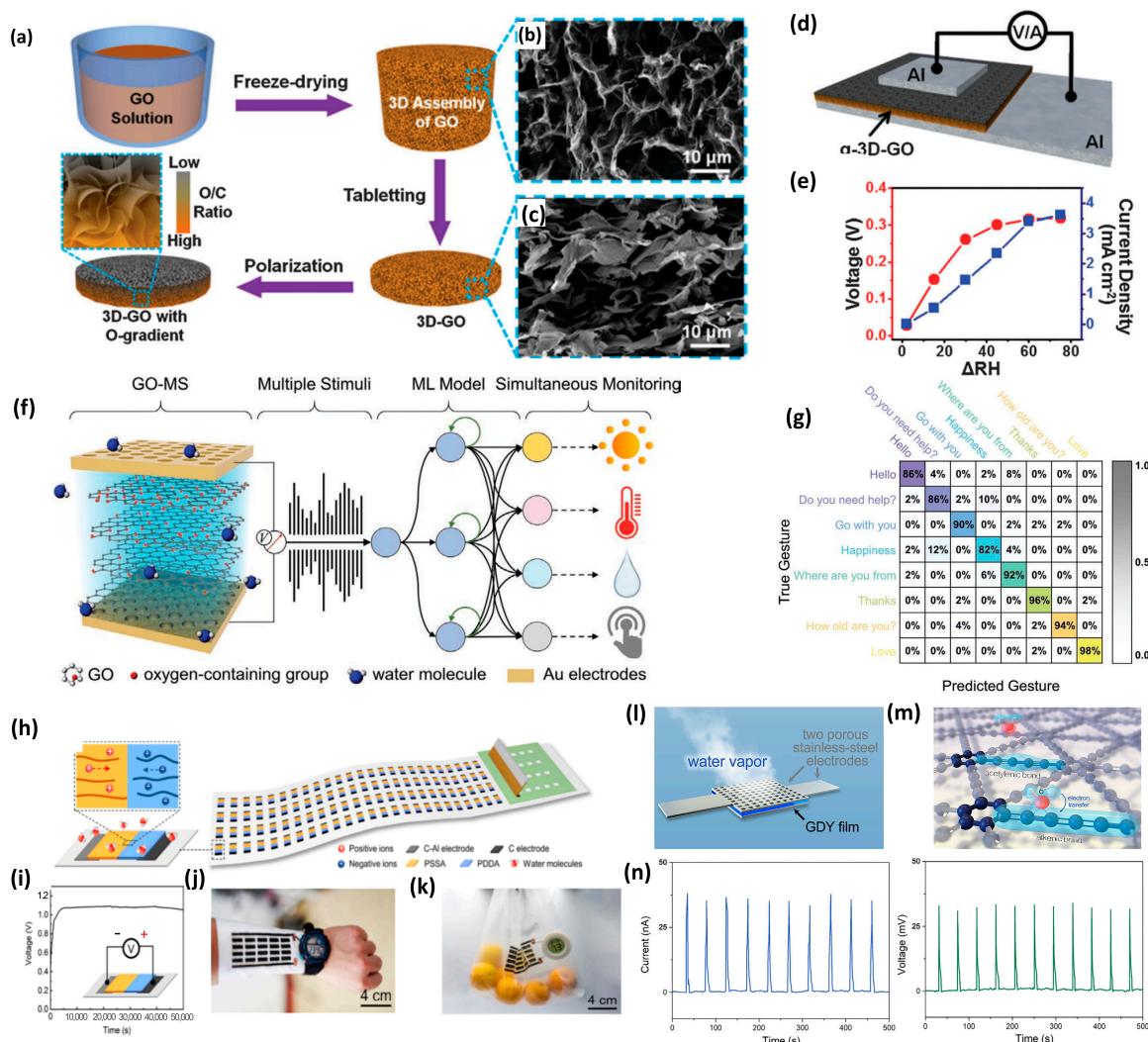

Figure 4. (**a**) Synthesis of 3D-GO via a three-step strategy. (**b**,**c**) Scanning electron microscopy (SEM) images of GO. (**d**) Schematic Representation of a moisture ion battery enclosed by Al electrodes. (**e**) Voltage and current outputs of moisture ion battery. (**f**) Schematic depiction of moisture ion batteries. (**g**) Integration with machine learning for precision information identification. (**h**) Composition of the moisture ion battery unit. (**i**) Continuous electrical signal emission from the unit for extended hours. (**j**,**k**) Practical application of moisture battery. (**l**) Schematic diagram of a device using GDY. (**m**) Mechanism schematic of acetylene bond transformation and electron transfer. (**n**) The GDY film device produces regular pulsed current signals upon intermittent stimulation.

Traditional devices relying on ME effect can generate the electrical signals through physical phenomena. GDY possesses a rich network of carbon-carbon triple bonds (acetylene bonds), an extensive conjugated structure, and adjustable electronic properties. Consequently, Chen et al. [87] pioneered the development of GDY-based moisture ion batteries. The device of the designed novel cell is illustrated in Figure 4l, where moisture sequentially pass through the top electrode, GDY membrane, and bottom electrode. This represents

a typical structure of a moisture ion battery. It adopts a sandwich structure composed of upper and lower electrodes with ME material in between. The top electrode is a metal electrode with micropores to allow moisture to enter. When moisture contacts the material, it releases charged particles that can migrate directionally. Due to the different contact times between the charged particles above and below the material, there is a concentration difference. As a result, the charged particles spontaneously move from high concentration to low concentration, generating an internal electric field. When the device is connected to an external circuit, it can generate voltage and current. Stable electrical signals can be generated at 90% relative humidity, as depicted in Figure 4n. When acetylene bonds encounter water vapor, they undergo a transformation into alkyne bonds. In this process, neutral water molecules carry positive charges as they migrate, resulting in the generation of an electrical signal in the external circuit (Figure 4m). This discovery has the potential for ME to be used for energy conversion and energy storage in the future.

3.2. Moisture Metal-Ion Batteries

A hydrogen ion has only one positive charge, so the ME generated by the hydrogen ion migration is limited. Therefore, researchers are gradually seeking high-valence ions to substitute hydrogen ions as moisture-generated carriers [84,88–91]. Chen et al. [92] employed electrochemical doping control technology, in which they successfully established a concentration gradient of high-valence metal cation carriers. As a result, high-valence Mg^{2+} and Al^{3+} are effectively incorporated into power generation materials. Mg^{2+} and Al^{3+} exhibit two-electron and three-electron transfer properties, leading to significant performance enhancements in ME.

Figure 5a depicts a schematic illustration of the moisture Mg ion and Al ion batteries. Metal-ion gradient-doped nanowires are positioned between two electrodes, with the upper electrode consisting of porous Au electrode. The insets elucidate the mechanism behind electrical signal generation. Charged ions dissociate upon exposure to moisture, moving in a specific direction, thereby producing ME. Experiments were conducted using materials containing sodium, magnesium, and aluminum ions (Figure 5b) to assess the impact of various charged ions on ME output. the current signal produced by aluminum ions was markedly higher than that of sodium ions, a disparity attributable to the greater charge density of aluminum ions. Simultaneously, it becomes evident that the moisture Na ion battery has the shortest duration, owing to variations in the diffusion rates of the metal cation carriers. In Figure 5c,d, under different RH, the ME signal of moisture aluminum ion battery is significantly higher than that of magnesium ion and sodium ion. These results highlight significantly higher output power in devices which can generate Mg^{2+} and Al^{3+} compared to those relying on Na^+ transport. In conclusion, high-valence ions that can move freely are more conducive to the output of ME signals.

In addition to creating an ion gradient by ionizing metal ions in ME materials, Sun et al. [93] introduced an active Zn electrode to develop a novel moisture metal ion battery. Figure 5e provides a schematic representation of the battery's fabrication. Conjugated electrospinning techniques were employed to encapsulate nanofibers of polyacrylonitrile onto zinc wires, each measuring several hundred micrometers in size. SEM image and EDS analysis of cross-sectional views of the fabricated fibers (Figure 5f,g) revealed the distribution of zinc within the fiber's core. The researchers conducted separate tests under various electrode conditions. The results indicated a significantly higher electrical signal output in the presence of the Zn electrode compared to the silver electrode, demonstrating the rationale for introducing the zinc electrode (Figure 5h). During this process, when the Zn electrode encounters moisture, a mild chemical reaction occurs, producing mobile Zn^{2+} (Figure 5i,j). On the Zn electrode side, the Zn^{2+} concentration surpasses that on the silver electrode side, creating a concentration gradient. Zn^{2+} spontaneously migrate from the high concentration side to the low concentration side. Additionally, due to the higher charge carried by Zn^{2+}, it contributes to the enhanced electrical signal output.
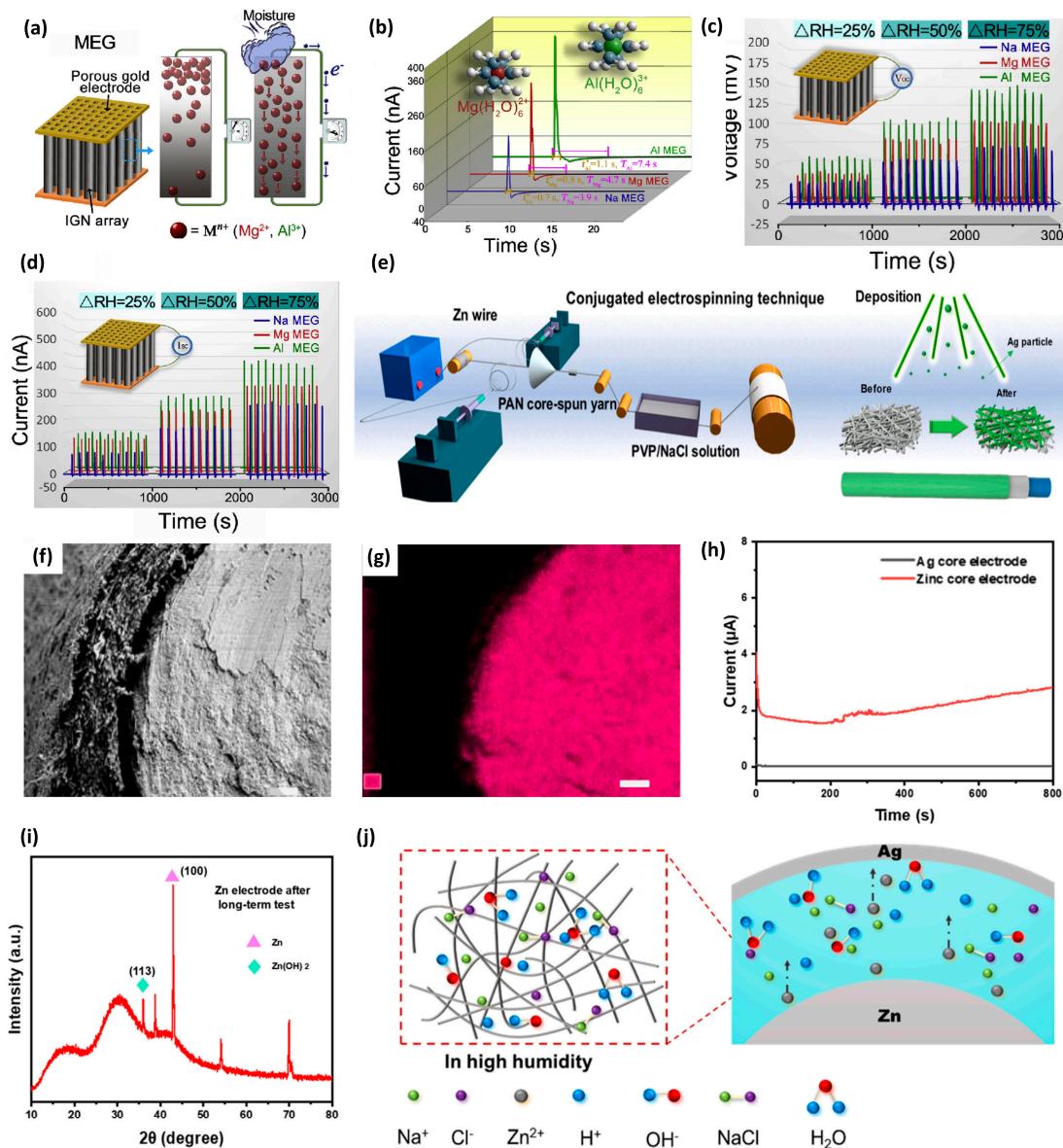
Figure 5. (**a**) Schematic diagram illustrates the moist−electric mechanism of Mg ME and Al ME. (**b**) Electrical signals produced by the different ions. (**c**) The output pulse voltage of materials with different charged ions under different changes in relative humidity environment. (**d**) The output pulse current of materials with different charged ions under different changes in relative humidity environment. (**e**) Diagram of the preparation process of moisture zinc ions batteries. (**f**) Cross−section SEM image of moisture metal ion batteries. (**g**) The corresponding energy dispersive spectroscopy (EDS) images of Zn element. (**h**) The current output when assembled with zinc as the core electrode or Ag as the core electrode. (**i**) XRD spectrum of zinc core electrode. (**j**) Electric generation mechanism in a high relative humidity.

3.3. Moisture Ion Batteries with Complex Structure

Moisture ion batteries are currently advancing towards complex and composite structures to broaden their application value. Huang et al. [94] has devised an intelligent solid moisture Mg ion battery (SMB). They introduced an intelligent SMB capable of responding to moisture and sunlight. They employed the emerging carbon allotrope, GDY, which can directly grow within a 3D melamine sponge, referred to as GDY/MS. As depicted in Figure 6a, GDY/MS serves as the SMB's cathode, simplifying the battery's construction, which only requires GDY/MS and Mg foil without the need for additional electrolytes or

separators. The operating principle of this battery involves a chemical bond conversion within GDY when it encounters moisture in the presence of electricity-producing materials. Simultaneously, chemical reactions occur between Mg and moisture, leading to an increase in electrical signal output. In addition, the moisture Mg ion battery can easily control light-emitting diode (LED) lights in a humid environment. Therefore, it can function as a switch for the automatic control of LED illumination by manipulating moisture levels in the surrounding atmosphere, as depicted in Figure 6b. Figure 6c reveals a direct correlation between battery voltage and environmental humidity. As humidity levels rise, so does the voltage. All these findings underscore innovative concepts and technologies for the production of intelligent batteries.
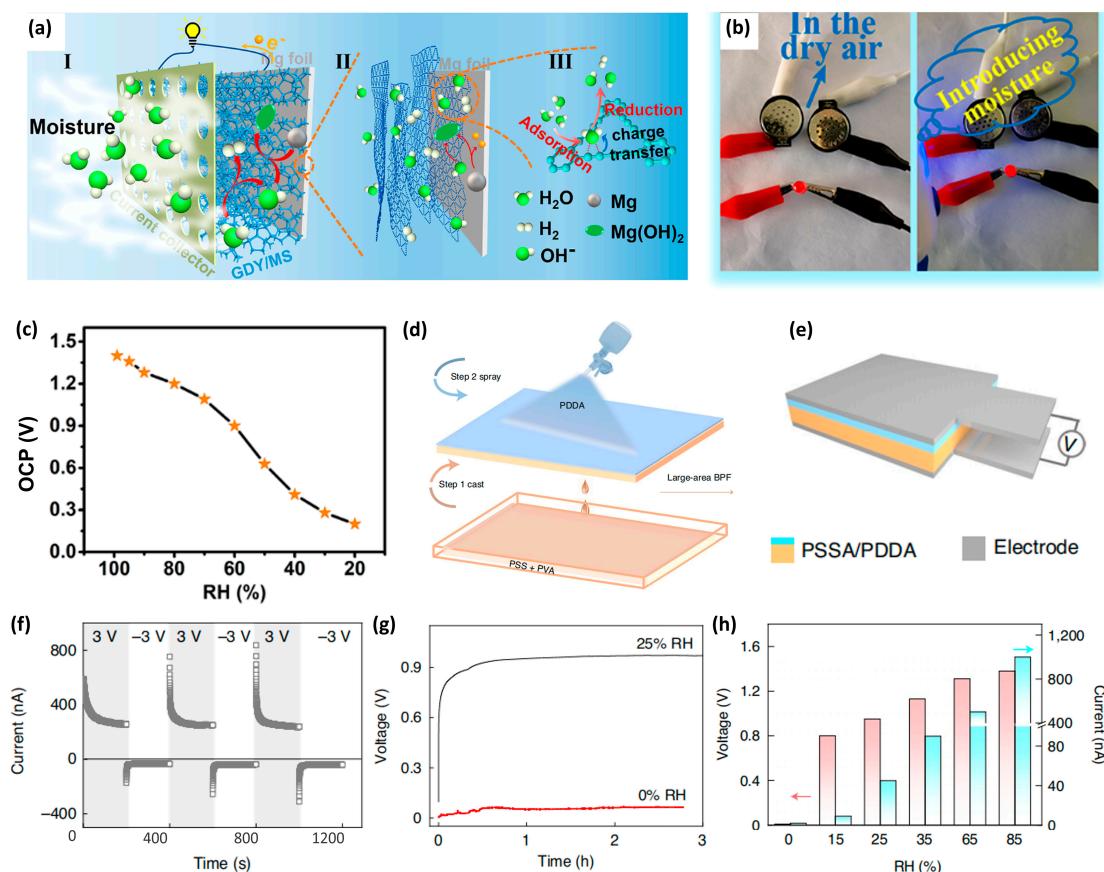

Figure 6. (**a**) Schematic diagram of the operational mechanism and electricity generation process of the battery. (**b**) The battery can illuminate LED within specific humidity conditions. (**c**) The relationship between battery output voltage and ambient humidity. (**d**) The BPF is prepared using a straightforward casting and spraying approach. The PSSA is created by casting a water-based blend of PSS and PVA, followed by the application of a PDDA suspension onto the PSSA film to obtain the BPF. (**e**) Schematic diagram of ion battery. (**f**) Current response of the ion battery under an alternating bias of ± 3 V (25% RH, 25 °C). (**g**) The voltage generated by the unit when exposed to air at 25% RH (black) and 0% RH (red). (**h**) Voltage and current output in response to variation in RH.

In the past, ME signals in moisture ion batteries were attributed to cation movement, driven by the inherent electric field within the ME materials. Subsequently, Wang et al. [95] drew inspiration from the asymmetric lipid bilayer structure. They proposed and designed a heterogeneous moisture ion battery utilizing double-layer polyelectrolyte films (BPFs) as the ME material. This design enabled the movement of both positively and negatively ions. As depicted in Figure 6d, BPF is prepared through a scalable and continuous casting and spraying process. To confirm that power generation results from bidirectional ion movement with opposite charges, a voltage of ± 3 V was applied to the device, and the

resulting electric current was measured (Figure 6e). The results demonstrate that the current signal differs when positive and negative voltages are applied, respectively. This provides evidence that the bilayer membrane contains mobile ions with opposing charges. To demonstrate the device's moisture responsiveness, its voltage was tested under varying humidity conditions. Voltage output is nearly negligible at RH $\approx$ 0%, but it can reach 0.9 V as relative humidity increases to 25% (Figure 6g). This is because, in the absence of moisture, the ions within the device remain undissociated. However, when the device encounters the moisture, the ions disassociate, resulting in the generation of an electrical signal. As shown in Figure 6f, an increase in RH leads to a gradual rise in both voltage and current values. At high RH, the ME output experiences a substantial increase due to heightened water adsorption and ion diffusion. It can reach a peak of approximately 1.38 V at RH 85% in the air (Figure 6h). All the aforementioned results illustrate innovative concepts and technologies for the production of intelligent batteries.

4. Summary and Prospects

In summary, we focus on the research outcomes of our group, summarizing the advancements in carbon-based batteries prepared through ion migration mechanisms. Subsequently, we provide a detailed introduction to our group's innovative self-powered moisture ion battery, driven by external stimuli like moisture, elucidating its operational principles and research progress. Energy storage and conversion devices based on ion migration encompass traditional storage batteries, such as LIBs, SIBs along with high-valence batteries like ZIBs, MIBs, and AIBs. Furthermore, as electrochemical energy devices undergo iterations, emerging self-generating batteries have been designed, which rely on ion migration and chemical energy conversion. The most typical of these is the moisture ion battery. Electrode materials representing carbon and its allotropes, as well as elements from Group-IV such as silicon, germanium, and tin, play an indispensable role in optimizing the performance of the aforementioned energy storage and conversion devices.

In the Group-IV elements, carbon exhibits a wide array of unique chemical structures, such as porous carbon, carbon nanotubes, graphene, and GDY. The diversity of carbon materials provides these ion migration-based batteries with a richer selection for energy storage or generation. Carbon materials feature numerous conductive pathways, allowing ions to swiftly traverse their interiors. As a result, the charging, discharging, or generation of ME signals in ion batteries is significantly accelerated, potentially enhancing the energy output of ion migration-based batteries. Furthermore, the abundant availability of carbon resources permits direct and cost-effective material synthesis, making it a pivotal component for improving the performance of energy devices and achieving commercial viability. Compared to carbon materials, Si-based materials offer advantages such as higher capacity, relatively lower charge–discharge plateaus, and abundant availability. Additionally, Ge-based materials exhibit superior electrical properties with higher charge carrier mobility. Exploring other Group-IV elements for ion migration-based batteries is a crucial driver for enhancing their performance.

Concerning energy devices designed based on ion migration mechanisms, two primary development directions exist. In the context of Group-IV materials traditional ion batteries, it is imperative to expand the exploration of new elements for battery applications. This expansion is crucial to mitigate potential limitations arising from Earth's finite resources in the battery industry. Simultaneously, it is essential to prioritize high ion migration efficiency within batteries and improve the overall energy utilization efficiency of battery equipment. Furthermore, in pursuit of these advancements, it is equally important to innovate more adaptable battery solutions, including flexible and micro-batteries, to address a broader range of application requirements. It is widely acknowledged that carbon materials are extensively used in battery anodes due to their high conductivity, hierarchical porous structures, and low cost. However, carbon materials also possess several drawbacks such as low specific capacity and poor rate performance. Hence, there is a necessity to broaden the exploration of new elements for battery applications. For instance, other elements, obtained

from diverse sources, offers higher theoretical energy density and lower material costs. Despite significant achievements made by numerous researchers in the field of batteries, challenges persist in enhancing energy density, improving safety, enabling rapid charging, and achieving high-power output.

In the context of emerging moisture ion batteries, the primary emphasis lies in improving the electrical output of individual devices and thoroughly exploring their potential applications. A secondary objective entails conducting comprehensive research on the performance of inorganic, organic, and composite materials in moisture ion batteries. Currently, the design of moisture ion battery devices is still in the exploratory phase, offering ample opportunities for innovation. Future designs should prioritize efficiency and customization to meet specific usage needs.

Conflicts of Interest: The authors declare no conflict of interest. They have no known competing financial interest or personal relationships that could have appeared to influence the work reported in this paper.

References

1. Song, Y.-C.; Woo, J.-H.; Oh, G.-G.; Kim, D.-H.; Lee, C.-Y.; Kim, H.-W. External electric field promotes ammonia stripping from wastewater. *Water Res.* **2021**, *203*, 117518. [CrossRef] [PubMed]
2. He, N.; Wang, H.; Li, F.; Jiang, B.; Tang, D.; Li, L. Ion engines in hydrogels boosting hydrovoltaic electricity generation. *Energy Environ. Sci.* **2023**, *16*, 2494–2504. [CrossRef]
3. Jacobs, D.A.; Wolff, C.M.; Chin, X.-Y.; Artuk, K.; Ballif, C.; Jeangros, Q. Lateral ion migration accelerates degradation in halide perovskite devices. *Energy Environ. Sci.* **2022**, *15*, 5324–5339. [CrossRef]
4. Lu, X.; Sun, Y.; Hu, W. The external electric field effect on the charge transport performance of organic semiconductors: A theoretical investigation. *J. Mater. Chem. A* **2021**, *9*, 21044–21050. [CrossRef]
5. Zhu, X.; Hao, J.; Bao, B.; Zhou, Y.; Zhang, H.; Pang, J.; Jiang, Z.; Jiang, L. Unique ion rectification in hypersaline environment: A high-performance and sustainable power generator system. *Sci. Adv.* **2018**, *4*, eaau1665. [CrossRef] [PubMed]
6. Zhang, W.; Sun, M.; Yin, J.; Abou-Hamad, E.; Schwingenschlögl, U.; Costa, P.M.F.J.; Alshareef, H.N. A Cyclized Polyacrylonitrile Anode for Alkali Metal Ion Batteries. *Angew. Chem. Int. Ed.* **2021**, *60*, 1355–1363. [CrossRef]
7. Li, Y.; Song, S.; Kim, H.; Nomoto, K.; Kim, H.; Sun, X.; Hori, S.; Suzuki, K.; Matsui, N.; Hirayama, M.; et al. A lithium superionic conductor for millimeter-thick battery electrode. *Science* **2023**, *381*, 50–53. [CrossRef]
8. Setiawan, D.; Kim, H.J.; Lyoo, J.; Hong, S.-T.; Chae, M.S. Novel layered iron vanadate as a stable high-voltage cathode material for nonaqueous magnesium-ion batteries. *Chem. Eng. J.* **2023**, *474*, 145596. [CrossRef]
9. Li, Y.; Jia, H.; Ali, U.; Wang, H.; Liu, B.; Li, L.; Zhang, L.; Wang, C. Successive Gradient Internal Electric Field Strategy toward Dendrite-Free Zinc Metal Anode. *Adv. Energy Mater.* **2023**, *13*, 2301643. [CrossRef]
10. Salanne, M.; Rotenberg, B.; Naoi, K.; Kaneko, K.; Taberna, P.-L.; Grey, C.P.; Dunn, B.; Simon, P. Efficient storage mechanisms for building better supercapacitors. *Nat. Energy* **2016**, *1*, 16070. [CrossRef]
11. González, A.; Goikolea, E.; Barrena, J.A.; Mysyk, R. Review on supercapacitors: Technologies and materials. *Renew. Sustain. Energy Rev.* **2016**, *58*, 1189–1206. [CrossRef]
12. Chen, G.Z. Supercapacitor and supercapattery as emerging electrochemical energy stores. *Int. Mater. Rev.* **2017**, *62*, 173–202. [CrossRef]
13. Liu, T.; Yan, R.; Huang, H.; Pan, L.; Cao, X.; deMello, A.; Niederberger, M. A Micromolding Method for Transparent and Flexible Thin-Film Supercapacitors and Hybrid Supercapacitors. *Adv. Funct. Mater.* **2020**, *30*, 2004410. [CrossRef]
14. Zhu, M.; Huang, Y.; Huang, Y.; Pei, Z.; Xue, Q.; Li, H.; Geng, H.; Zhi, C. Capacitance Enhancement in a Semiconductor Nanostructure-Based Supercapacitor by Solar Light and a Self-Powered Supercapacitor–Photodetector System. *Adv. Funct. Mater.* **2016**, *26*, 4481–4490. [CrossRef]
15. Qin, H.; Liu, P.; Chen, C.; Cong, H.-P.; Yu, S.-H. A multi-responsive healable supercapacitor. *Nat. Commun.* **2021**, *12*, 4297. [CrossRef] [PubMed]
16. Flores-Diaz, N.; De Rossi, F.; Das, A.; Deepa, M.; Brunetti, F.; Freitag, M. Progress of Photocapacitors. *Chem. Rev.* **2023**, *123*, 9327–9355. [CrossRef]
17. Yi, F.; Ren, H.; Dai, K.; Wang, X.; Han, Y.; Wang, K.; Li, K.; Guan, B.; Wang, J.; Tang, M.; et al. Solar thermal-driven capacitance enhancement of supercapacitors. *Energy Environ. Sci.* **2018**, *11*, 2016–2024. [CrossRef]
18. Zhao, D.; Wang, H.; Khan, Z.U.; Chen, J.C.; Gabrielsson, R.; Jonsson, M.P.; Berggren, M.; Crispin, X. Ionic thermoelectric supercapacitors. *Energy Environ. Sci.* **2016**, *9*, 1450–1457. [CrossRef]

19. Hoffmann, M.; Fengler, F.P.G.; Max, B.; Schroeder, U.; Slesazeck, S.; Mikolajick, T. Negative Capacitance for Electrostatic Supercapacitors. *Adv. Energy Mater.* **2019**, *9*, 1901154. [CrossRef]

20. Yang, Y.; Li, P.; Zheng, X.; Sun, W.; Dou, S.X.; Ma, T.; Pan, H. Anion-exchange membrane water electrolyzers and fuel cells. *Chem. Soc. Rev.* **2022**, *51*, 9620–9693. [CrossRef]

21. Farooqui, U.R.; Ahmad, A.L.; Hamid, N.A. Graphene oxide: A promising membrane material for fuel cells. *Renew. Sustain. Energy Rev.* **2018**, *82*, 714–733. [CrossRef]

22. Wang, Y.; Ruiz Diaz, D.F.; Chen, K.S.; Wang, Z.; Adroher, X.C. Materials, technological status, and fundamentals of PEM fuel cells—A review. *Mater. Today* **2020**, *32*, 178–203. [CrossRef]

23. Yurko, Y.; Elbaz, L. Direct Quinone Fuel Cells. *J. Am. Chem. Soc.* **2023**, *145*, 2653–2660. [CrossRef] [PubMed]

24. Ren, Z.J. Microbial fuel cells: Running on gas. *Nat. Energy* **2017**, *2*, 17093. [CrossRef]

25. Xiao, F.; Wang, Y.; Wu, Z.; Chen, G.; Yang, F.; Zhu, S.; Siddharth, K.; Kong, Z.; Lu, A.; Li, J.; et al. Recent Advances in Electrocatalysts for Proton Exchange Membrane Fuel Cells and Alkaline Membrane Fuel Cells. *Adv. Mater.* **2021**, *33*, 2006292. [CrossRef]

26. Li, W.; Wang, D.; Zhang, Y.; Tao, L.; Wang, T.; Zou, Y.; Wang, Y.; Chen, R.; Wang, S. Defect Engineering for Fuel-Cell Electrocatalysts. *Adv. Mater.* **2020**, *32*, 1907879. [CrossRef] [PubMed]

27. Duan, C.; Kee, R.J.; Zhu, H.; Karakaya, C.; Chen, Y.; Ricote, S.; Jarry, A.; Crumlin, E.J.; Hook, D.; Braun, R.; et al. Highly durable, coking and sulfur tolerant, fuel-flexible protonic ceramic fuel cells. *Nature* **2018**, *557*, 217–222. [CrossRef] [PubMed]

28. Fukuzumi, S. Production of Liquid Solar Fuels and Their Use in Fuel Cells. *Joule* **2017**, *1*, 689–738. [CrossRef]

29. Zaman, S.; Huang, L.; Douka, A.I.; Yang, H.; You, B.; Xia, B.Y. Oxygen Reduction Electrocatalysts toward Practical Fuel Cells: Progress and Perspectives. *Angew. Chem. Int. Ed.* **2021**, *60*, 17832–17852. [CrossRef]

30. Zhang, L.; Wang, W.; Lu, S.; Xiang, Y. Carbon Anode Materials: A Detailed Comparison between Na-ion and K-ion Batteries. *Adv. Energy Mater.* **2021**, *11*, 2003640. [CrossRef]

31. Zhao, L.; Hu, Z.; Lai, W.; Tao, Y.; Peng, J.; Miao, Z.; Wang, Y.; Chou, S.; Liu, H.; Dou, S. Hard Carbon Anodes: Fundamental Understanding and Commercial Perspectives for Na-Ion Batteries beyond Li-Ion and K-Ion Counterparts. *Adv. Energy Mater.* **2021**, *11*, 2002704. [CrossRef]

32. Wang, G.; Yu, M.; Feng, X. Carbon materials for ion-intercalation involved rechargeable battery technologies. *Chem. Soc. Rev.* **2021**, *50*, 2388–2443. [CrossRef] [PubMed]

33. Quertite, K.; Enriquez, H.; Trcera, N.; Tong, Y.; Bendounan, A.; Mayne, A.J.; Dujardin, G.; Lagarde, P.; El Kenz, A.; Benyoussef, A.; et al. Silicene Nanoribbons on an Insulating Thin Film. *Adv. Funct. Mater.* **2021**, *31*, 2007013. [CrossRef]

34. Martella, C.; Massetti, C.; Dhungana, D.S.; Bonera, E.; Grazianetti, C.; Molle, A. Bendable Silicene Membranes. *Adv. Mater.* **2023**, *35*, 2211419. [CrossRef] [PubMed]

35. Zhuang, J.; Gao, N.; Li, Z.; Xu, X.; Wang, J.; Zhao, J.; Dou, S.X.; Du, Y. Cooperative Electron–Phonon Coupling and Buckled Structure in Germanene on Au(111). *ACS Nano* **2017**, *11*, 3553–3559. [CrossRef] [PubMed]

36. Chen, H.; Guo, F.; Liu, Y.; Huang, T.; Zheng, B.; Ananth, N.; Xu, Z.; Gao, W.; Gao, C. A Defect-Free Principle for Advanced Graphene Cathode of Aluminum-Ion Battery. *Adv. Mater.* **2017**, *29*, 1605958. [CrossRef] [PubMed]

37. Wang, J.; Wang, J.; Liu, H.; You, Z.; Li, Z.; Kang, F.; Wei, B. A Highly Flexible and Lightweight MnO_2/Graphene Membrane for Superior Zinc-Ion Batteries. *Adv. Funct. Mater.* **2021**, *31*, 2007397. [CrossRef]

38. Hu, Y.; Luo, B.; Ye, D.; Zhu, X.; Lyu, M.; Wang, L. An Innovative Freeze-Dried Reduced Graphene Oxide Supported SnS_2 Cathode Active Material for Aluminum-Ion Batteries. *Adv. Mater.* **2017**, *29*, 1606132. [CrossRef]

39. Zhou, Y.; Zhu, Y.; Xu, B.; Zhang, X.; Al-Ghanim, K.A.; Mahboob, S. Cobalt Sulfide Confined in N-Doped Porous Branched Carbon Nanotubes for Lithium-Ion Batteries. *Nano-Micro Lett.* **2019**, *11*, 29. [CrossRef]

40. Fan, L.; Ma, R.; Zhang, Q.; Jia, X.; Lu, B. Graphite Anode for a Potassium-Ion Battery with Unprecedented Performance. *Angew. Chem. Int. Ed.* **2019**, *58*, 10500–10505. [CrossRef]

41. Pang, Q.; Sun, C.; Yu, Y.; Zhao, K.; Zhang, Z.; Voyles, P.M.; Chen, G.; Wei, Y.; Wang, X. $H_2V_3O_8$ Nanowire/Graphene Electrodes for Aqueous Rechargeable Zinc Ion Batteries with High Rate Capability and Large Capacity. *Adv. Energy Mater.* **2018**, *8*, 1800144. [CrossRef]

42. Share, K.; Cohn, A.P.; Carter, R.; Rogers, B.; Pint, C.L. Role of Nitrogen-Doped Graphene for Improved High-Capacity Potassium Ion Battery Anodes. *ACS Nano* **2016**, *10*, 9738–9744. [CrossRef] [PubMed]

43. Shen, D.; Duley, W.W.; Peng, P.; Xiao, M.; Feng, J.; Liu, L.; Zou, G.; Zhou, Y.N. Moisture-Enabled Electricity Generation: From Physics and Materials to Self-Powered Applications. *Adv. Mater.* **2020**, *32*, 2003722. [CrossRef] [PubMed]

44. Xu, J.; Li, T.; Yan, T.; Wu, S.; Wu, M.; Chao, J.; Huo, X.; Wang, P.; Wang, R. Ultrahigh solar-driven atmospheric water production enabled by scalable rapid-cycling water harvester with vertically aligned nanocomposite sorbent. *Energy Environ. Sci.* **2021**, *14*, 5979–5994. [CrossRef]

45. Zhao, F.; Cheng, H.; Zhang, Z.; Jiang, L.; Qu, L. Direct Power Generation from a Graphene Oxide Film under Moisture. *Adv. Mater.* **2015**, *27*, 4351–4357. [CrossRef] [PubMed]

46. Zhao, Z.; Das, S.; Xing, G.; Fayon, P.; Heasman, P.; Jay, M.; Bailey, S.; Lambert, C.; Yamada, H.; Wakihara, T.; et al. A 3D Organically Synthesized Porous Carbon Material for Lithium-Ion Batteries. *Angew. Chem. Int. Ed.* **2018**, *57*, 11952–11956. [CrossRef]

47. Niu, J.; Shao, R.; Liang, J.; Dou, M.; Li, Z.; Huang, Y.; Wang, F. Biomass-derived mesopore-dominant porous carbons with large specific surface area and high defect density as high performance electrode materials for Li-ion batteries and supercapacitors. *Nano Energy* **2017**, *36*, 322–330. [CrossRef]

48. Gao, F.; Geng, C.; Xiao, N.; Qu, J.; Qiu, J. Hierarchical porous carbon sheets derived from biomass containing an activation agent and in-built template for lithium ion batteries. *Carbon* **2018**, *139*, 1085–1092. [CrossRef]

49. Liu, S.; Lin, Z.; Xiao, F.; Zhang, J.; Wang, D.; Chen, X.; Zhao, Y.; Xu, J. Co-N-C in porous carbon with enhanced lithium ion storage properties. *Chem. Eng. J.* **2020**, *389*, 124377. [CrossRef]

50. Chen, X.; Li, Z.; Li, Y.; Shen, C.; Zhou, C.; Tan, X.; Yan, K.; Zhang, G.; Xu, X. Carbon Nanotube Interwoven Polyhedrons with Inside-out Lithiophilic Gradients toward Stable Lithium Metal Battery. *Chem. Eng. J.* **2022**, *442*, 136256. [CrossRef]

51. Abdul Razzaq, A.; Yao, Y.; Shah, R.; Qi, P.; Miao, L.; Chen, M.; Zhao, X.; Peng, Y.; Deng, Z. High-performance lithium sulfur batteries enabled by a synergy between sulfur and carbon nanotubes. *Energy Storage Mater.* **2019**, *16*, 194–202. [CrossRef]

52. Yang, G.; Liu, Z.; Weng, S.; Zhang, Q.; Wang, X.; Wang, Z.; Gu, L.; Chen, L. Iron carbide allured lithium metal storage in carbon nanotube cavities. *Energy Storage Mater.* **2021**, *36*, 459–465. [CrossRef]

53. Pan, Z.; Ren, J.; Guan, G.; Fang, X.; Wang, B.; Doo, S.-G.; Son, I.H.; Huang, X.; Peng, H. Synthesizing Nitrogen-Doped Core-Sheath Carbon Nanotube Films for Flexible Lithium Ion Batteries. *Adv. Energy Mater.* **2016**, *6*, 1600271. [CrossRef]

54. Kühne, M.; Börrnert, F.; Fecher, S.; Ghorbani-Asl, M.; Biskupek, J.; Samuelis, D.; Krasheninnikov, A.V.; Kaiser, U.; Smet, J.H. Reversible superdense ordering of lithium between two graphene sheets. *Nature* **2018**, *564*, 234–239. [CrossRef] [PubMed]

55. Tao, R.; Li, F.; Lu, X.; Liu, F.; Xu, J.; Kong, D.; Zhang, C.; Tan, X.; Ma, S.; Shi, W.; et al. High-Conductivity–Dispersibility Graphene Made by Catalytic Exfoliation of Graphite for Lithium-Ion Battery. *Adv. Funct. Mater.* **2021**, *31*, 2007630. [CrossRef]

56. Fan, Q.; Noh, H.-J.; Wei, Z.; Zhang, J.; Lian, X.; Ma, J.; Jung, S.-M.; Jeon, I.-Y.; Xu, J.; Baek, J.-B. Edge-thionic acid-functionalized graphene nanoplatelets as anode materials for high-rate lithium ion batteries. *Nano Energy* **2019**, *62*, 419–425. [CrossRef]

57. Zhang, J.; Ai, Y.; Wu, J.; Zhang, D.; Wang, Y.; Feng, Z.; Sun, H.; Liang, Q.; Sun, T.; Yang, Y. Nickel-Catalyzed Synthesis of 3D Edge-Curled Graphene for High-Performance Lithium-Ion Batteries. *Adv. Funct. Mater.* **2020**, *30*, 1904645. [CrossRef]

58. Wang, N.; He, J.; Tu, Z.; Yang, Z.; Zhao, F.; Li, X.; Huang, C.; Wang, K.; Jiu, T.; Yi, Y.; et al. Synthesis of Chlorine-Substituted Graphdiyne and Applications for Lithium-Ion Storage. *Angew. Chem. Int. Ed.* **2017**, *56*, 10740–10745. [CrossRef]

59. Zhao, Y.; Zhu, J.; Ong, S.J.H.; Yao, Q.; Shi, X.; Hou, K.; Xu, Z.J.; Guan, L. High-Rate and Ultralong Cycle-Life Potassium Ion Batteries Enabled by In Situ Engineering of Yolk–Shell FeS_2@C Structure on Graphene Matrix. *Adv. Energy Mater.* **2018**, *8*, 1802565. [CrossRef]

60. Sun, J.; Sadd, M.; Edenborg, P.; Grönbeck, H.; Thiesen, P.H.; Xia, Z.; Quintano, V.; Qiu, R.; Matic, A.; Palermo, V. Real-time imaging of Na^+ reversible intercalation in "Janus" graphene stacks for battery applications. *Sci. Adv.* **2021**, *7*, eabf0812. [CrossRef]

61. Zhao, D.; Zhang, Z.; Ren, J.; Xu, Y.; Xu, X.; Zhou, J.; Gao, F.; Tang, H.; Liu, S.; Wang, Z.; et al. Fe_2VO_4 nanoparticles on rGO as anode material for high-rate and durable lithium and sodium ion batteries. *Chem. Eng. J.* **2023**, *451*, 138882. [CrossRef]

62. Yi, Y.; Li, J.; Zhao, W.; Zeng, Z.; Lu, C.; Ren, H.; Sun, J.; Zhang, J.; Liu, Z. Temperature-Mediated Engineering of Graphdiyne Framework Enabling High-Performance Potassium Storage. *Adv. Funct. Mater.* **2020**, *30*, 2003039. [CrossRef]

63. Wang, N.; Li, X.; Tu, Z.; Zhao, F.; He, J.; Guan, Z.; Huang, C.; Yi, Y.; Li, Y. Synthesis and Electronic Structure of Boron-Graphdiyne with an sp-Hybridized Carbon Skeleton and Its Application in Sodium Storage. *Angew. Chem. Int. Ed.* **2018**, *57*, 3968–3973. [CrossRef] [PubMed]

64. Ge, J.; Wang, B.; Zhou, J.; Liang, S.; Rao, A.M.; Lu, B. Hierarchically Structured Nitrogen-Doped Carbon Microspheres for Advanced Potassium Ion Batteries. *ACS Mater. Lett.* **2020**, *2*, 853–860. [CrossRef]

65. Ge, J.; Fan, L.; Wang, J.; Zhang, Q.; Liu, Z.; Zhang, E.; Liu, Q.; Yu, X.; Lu, B. $MoSe_2$/N-Doped Carbon as Anodes for Potassium-Ion Batteries. *Adv. Energy Mater.* **2018**, *8*, 1801477. [CrossRef]

66. Xie, J.; Li, C.; Cui, Z.; Guo, X. Transition-Metal-Free Magnesium-Based Batteries Activated by Anionic Insertion into Fluorinated Graphene Nanosheets. *Adv. Funct. Mater.* **2015**, *25*, 6519–6526. [CrossRef]

67. Wang, J.; Zhang, Y.; Liu, G.; Zhang, T.; Zhang, C.; Zhang, Y.; Feng, Y.; Chi, Q. Improvements in the Magnesium Ion Transport Properties of Graphene/CNT-Wrapped TiO_2-B Nanoflowers by Nickel Doping. *Small* **2023**, *19*, 2304969. [CrossRef] [PubMed]

68. Luo, P.; Xiao, Y.; Yang, J.; Zuo, C.; Xiong, F.; Tang, C.; Liu, G.; Zhang, W.; Tang, W.; Wang, S.; et al. Polyaniline nanoarrays/carbon cloth as binder-free and flexible cathode for magnesium ion batteries. *Chem. Eng. J.* **2022**, *433*, 133772. [CrossRef]

69. Zhang, X.; Tang, Y.; He, P.; Zhang, Z.; Chen, T. Edge-rich vertical graphene nanosheets templating V_2O_5 for highly durable zinc ion battery. *Carbon* **2021**, *172*, 207–213. [CrossRef]

70. Qiu, N.; Yang, Z.; Xue, R.; Wang, Y.; Zhu, Y.; Liu, W. Toward a High-Performance Aqueous Zinc Ion Battery: Potassium Vanadate Nanobelts and Carbon Enhanced Zinc Foil. *Nano Lett.* **2021**, *21*, 2738–2744. [CrossRef]

71. Wang, X.; Wang, L.; Zhang, B.; Feng, J.; Zhang, J.; Ou, X.; Hou, F.; Liang, J. A flexible carbon nanotube@V_2O_5 film as a high-capacity and durable cathode for zinc ion batteries. *J. Energy Chem.* **2021**, *59*, 126–133. [CrossRef]

72. Guo, Q.; Wang, H.; Sun, X.; Yang, Y.; Chen, N.; Qu, L. In Situ Synthesis of Cathode Materials for Aqueous High-Rate and Durable $Zn–I_2$ Batteries. *ACS Mater. Lett.* **2022**, *4*, 1872–1881. [CrossRef]

73. Wang, X.; Gao, J.; Cheng, Z.; Chen, N.; Qu, L. A Responsive Battery with Controlled Energy Release. *Angew. Chem. Int. Ed.* **2016**, *55*, 14643–14647. [CrossRef]

74. Huang, H.; Zhou, F.; Shi, X.; Qin, J.; Zhang, Z.; Bao, X.; Wu, Z.-S. Graphene aerogel derived compact films for ultrafast and high-capacity aluminum ion batteries. *Energy Storage Mater.* **2019**, *23*, 664–669. [CrossRef]

75. Kong, Y.; Tang, C.; Huang, X.; Nanjundan, A.K.; Zou, J.; Du, A.; Yu, C. Thermal Reductive Perforation of Graphene Cathode for High-Performance Aluminum-Ion Batteries. *Adv. Funct. Mater.* **2021**, *31*, 2010569. [CrossRef]

76. Zhang, J.; Zhang, L.; Zhao, Y.; Meng, J.; Wen, B.; Muttaqi, K.M.; Islam, M.R.; Cai, Q.; Zhang, S. High-Performance Rechargeable Aluminum-Ion Batteries Enabled by Composite FeF_3 @ Expanded Graphite Cathode and Carbon Nanotube-Modified Separator. *Adv. Energy Mater.* **2022**, *12*, 2200959. [CrossRef]

77. Yu, X.; Zhao, G.; Huang, H.; Liu, C.; Lyu, P.; Zhang, N. Interlayer-expanded MoS_2 nanoflowers anchored on the graphene: A high-performance Li^+/Mg^{2+} co-intercalation cathode material. *Chem. Eng. J.* **2022**, *428*, 131214. [CrossRef]

78. Shen, H.; An, Y.; Man, Q.; Wang, J.; Liu, C.; Xi, B.; Xiong, S.; Feng, J.; Qian, Y. Controlled prelithiation of siloxene nanosheet anodes enables high performance 5 V-class lithium-ion batteries. *Chem. Eng. J.* **2023**, *454*, 140136. [CrossRef]

79. Mu, T.; Xiang, L.; Wan, X.; Lou, S.; Du, C.; Zuo, P.; Yin, G. Ultrahigh areal capacity silicon anodes realized via manipulating electrode structure. *Energy Storage Mater.* **2022**, *53*, 958–968. [CrossRef]

80. Liu, H.; Wu, T.; Zhang, L.; Wang, X.; Li, H.; Liu, S.; Zhang, Q.; Zhang, X.; Yu, H. Germanium Nanowires via Molten-Salt Electrolysis for Lithium Battery Anode. *ACS Nano* **2022**, *16*, 14402–14411. [CrossRef] [PubMed]

81. Guo, Q.; Yang, Y.; Wang, L.; Chen, N.; Qu, L. The Feasible Design of Quasi-Solid-State Aqueous Tin-Iodine Batteries. *Renewables* **2023**, *1*, 474–483. [CrossRef]

82. Yuan, L.; Xiao, X.; Ding, T.; Zhong, J.; Zhang, X.; Shen, Y.; Hu, B.; Huang, Y.; Zhou, J.; Wang, Z.L. Paper-Based Supercapacitors for Self-Powered Nanosystems. *Angew. Chem.* **2012**, *124*, 5018–5022. [CrossRef]

83. Zhao, D.; Zhu, Y.; Cheng, W.; Chen, W.; Wu, Y.; Yu, H. Cellulose-Based Flexible Functional Materials for Emerging Intelligent Electronics. *Adv. Mater.* **2021**, *33*, 2000619. [CrossRef]

84. Zhao, F.; Liang, Y.; Cheng, H.; Jiang, L.; Qu, L. Highly efficient moisture-enabled electricity generation from graphene oxide frameworks. *Energy Environ. Sci.* **2016**, *9*, 912–916. [CrossRef]

85. Yang, C.; Wang, H.; Yang, J.; Yao, H.; He, T.; Bai, J.; Guang, T.; Cheng, H.; Yan, J.; Qu, L. A Machine-Learning-Enhanced Simultaneous and Multimodal Sensor Based on Moist-Electric Powered Graphene Oxide. *Adv. Mater.* **2022**, *34*, 2205249. [CrossRef]

86. He, T.; Wang, H.; Lu, B.; Guang, T.; Yang, C.; Huang, Y.; Cheng, H.; Qu, L. Fully printed planar moisture-enabled electric generator arrays for scalable function integration. *Joule* **2023**, *7*, 935–951. [CrossRef]

87. Chen, N.; Yang, Y.; He, F.; Li, Y.; Liu, Q.; Li, Y. Chemical bond conversion directly drives power generation on the surface of graphdiyne. *Matter* **2022**, *5*, 2933–2945. [CrossRef]

88. Liang, Y.; Zhao, F.; Cheng, Z.; Zhou, Q.; Shao, H.; Jiang, L.; Qu, L. Self-powered wearable graphene fiber for information expression. *Nano Energy* **2017**, *32*, 329–335. [CrossRef]

89. Liang, Y.; Zhao, F.; Cheng, Z.; Deng, Y.; Xiao, Y.; Cheng, H.; Zhang, P.; Huang, Y.; Shao, H.; Qu, L. Electric power generation via asymmetric moisturizing of graphene oxide for flexible, printable and portable electronics. *Energy Environ. Sci.* **2018**, *11*, 1730–1735. [CrossRef]

90. Cheng, H.; Huang, Y.; Zhao, F.; Yang, C.; Zhang, P.; Jiang, L.; Shi, G.; Qu, L. Spontaneous power source in ambient air of a well-directionally reduced graphene oxide bulk. *Energy Environ. Sci.* **2018**, *11*, 2839–2845. [CrossRef]

91. Xu, T.; Ding, X.; Huang, Y.; Shao, C.; Song, L.; Gao, X.; Zhang, Z.; Qu, L. An efficient polymer moist-electric generator. *Energy Environ. Sci.* **2019**, *12*, 972–978. [CrossRef]

92. Chen, N.; Liu, Q.; Liu, C.; Zhang, G.; Jing, J.; Shao, C.; Han, Y.; Qu, L. MEG actualized by high-valent metal carrier transport. *Nano Energy* **2019**, *65*, 104047. [CrossRef]

93. Sun, Z.; Wen, X.; Guo, S.; Zhou, M.; Wang, L.; Qin, X.; Tan, S.C. Weavable yarn-shaped moisture-induced electric generator. *Nano Energy* **2023**, *116*, 108748. [CrossRef]

94. Fu, X.; He, F.; Gao, J.; Yan, X.; Chang, Q.; Zhang, Z.; Huang, C.; Li, Y. Directly Growing Graphdiyne Nanoarray Cathode to Integrate an Intelligent Solid Mg-Moisture Battery. *J. Am. Chem. Soc.* **2023**, *145*, 2759–2764. [CrossRef]

95. Wang, H.; Sun, Y.; He, T.; Huang, Y.; Cheng, H.; Li, C.; Xie, D.; Yang, P.; Zhang, Y.; Qu, L. Bilayer of polyelectrolyte films for spontaneous power generation in air up to an integrated 1000 V output. *Nat. Nanotechnol.* **2021**, *16*, 811–819. [CrossRef]